Shape-Enhanced Photocatalytic Activity of Single-Crystalline Anatase TiO$_2$ (101) Nanobelts

Nianqiang Wu,*,[†] Jin Wang,[†] De Nyago Tafen,[‡] Hong Wang,[‡] Jian-Guo Zheng,[§]
James P. Lewis,[‡] Xiaogang Liu,[⊥] Stephen S. Leonard,[ǁ] and
Ayyakkannu Manivannan[△]

*Department of Mechanical and Aerospace Engineering, WVNano Initiative, West Virginia
University, Morgantown, West Virginia 26506-6106, Department of Physics, West Virginia
University, Morgantown, West Virginia 26506, Materials Characterization Center (MC2), LEXI,
California Institute for Telecommunication and Information Technology, University of
California, Irvine, California 92697, Department of Chemistry, National University of
Singapore, Singapore 117543, National Institute for Occupational Safety and Health,
Morgantown, West Virginia 26505, and National Energy Technology Laboratory, U.S.
Department of Energy, Morgantown, West Virginia 26507*

Received November 7, 2009; E-mail: nick.wu@mail.wvu.edu

Abstract: Particle size is generally considered to be the primary factor in the design of nanocrystal photocatalysts, because the reduction of particle size increases the number of active sites. However, the benefit from the size reduction can be canceled by a higher electron−hole recombination rate due to the confined space in sphere-shaped nanoparticles. Here we report a mechanistic study on a novel nanobelt structure that overcomes the drawback of sphere-shaped nanoparticles. Single-crystalline anatase TiO$_2$ nanobelts with two dominant surfaces of (101) facet exhibit enhanced photocatalytic activity over the nanosphere counterparts with an identical crystal phase and similar specific surface area. The *ab initio* density functional theory (DFT) calculations show that the exposed (101) facet of the nanobelts yields an enhanced reactivity with molecular O$_2$, facilitating the generation of superoxide radical. Moreover, the nanobelts exhibit a lower electron−hole recombination rate than the nanospheres due to the following three reasons: (i) greater charge mobility in the nanobelts, which is enabled along the longitudinal dimension of the crystals; (ii) fewer localized states near the band edges and in the bandgap due to fewer unpassivated surface states in the nanobelts; and (iii) enhanced charge separation due to trapping of photogenerated electrons by chemisorbed molecular O$_2$ on the (101) facet. Our results suggest that the photocatalysis efficiency of nanocrystals can be significantly improved by tailoring the shape and the surface structure of nanocrystals, which provides a new concept for rational design and development of high-performance photocatalysts.

1. Introduction

Titanium oxide photocatalysts are of great importance due to increasing applications in hydrogen generation, solar energy utilization, environmental remediation, and biomedical applications.[1−4] Photocatalysis of TiO$_2$ generally involves four processes:[1−4] (i) generation of electrons and holes by photoexcitation; (ii) migration of the photogenerated charge carriers to the surface; (iii) subsequent reduction/oxidization of the adsorbed reactants directly by electrons/holes or by reactive oxygen species (ROS); and (iv) recombination of the photogenerated electron−hole pairs. Desired photocatalysts are expected to promote processes (i), (ii), and (iii) while suppressing process (iv). Smaller particles are generally preferred as photocatalysts due to higher specific surface area, leading to more surface reactive sites. However, for commonly used sphere-shaped nanoparticles (called nanospheres), the benefit from the size reduction would be canceled by a higher electron−hole recombination rate,[5] because the photogenerated electrons and holes may not be efficiently separated from each other in the confined space.[6] Recent studies have shown that the geometry of nanoparticles has a significant effect on the photoelectrolysis activity.[7] TiO$_2$ nanotubes act as electron highways that exhibit superior electron transport capability in dye-sensitized solar cells.[8,9] We postulate that one-dimensional (1-D) single-

† Department of Mechanical and Aerospace Engineering, West Virginia University.
‡ Department of Physics, West Virginia University.
§ University of California.
⊥ National University of Singapore.
ǁ National Institute for Occupational Safety and Health.
△ National Energy Technology Laboratory.
(1) Hoffmann, M. R.; Martin, S. T.; Choi, W. *Chem. Rev.* **1995**, *95*, 69.
(2) Linsebigler, A. L.; Lu, G. Q.; Yates, J. T. *Chem. Rev.* **1995**, *95*, 735.
(3) Mills, A.; Le Hunte, S. J. *Photochem. Photobiol. A* **1997**, *108*, 1.
(4) Fujishima, A.; Zhang, X. T.; Tryk, D. A. *Surf. Sci. Rep.* **2008**, *63*, 515.
(5) Grela, M. A.; Colussi, A. J. *J. Phys. Chem.* **1996**, *100*, 18214.
(6) Murakami, N.; Kurihara, Y.; Tsubota, T.; Ohno, T. *J. Phys. Chem. C* **2009**, *113*, 3062.
(7) Mor, G. K.; Shankar, K.; Paulose, M.; Grimes, C. A. *Nano Lett.* **2005**, *5*, 191.
(8) Gopal, K.; Mor, G. K.; Shankar, K.; Paulose, M.; Varghese, O. K.; Grimes, C. A. *Nano Lett.* **2006**, *6*, 215.

crystalline nanostructures such as nanobelts, nanowires, and nanotubes would retain high specific surface area but have a lower charge carrier recombination rate as compared to nanospheres. This postulation was built on a hypothesis that charge carriers are less localized in 1-D nanostructured single crystals where the photogenerated electrons and holes are free to transport throughout the whole length dimension of the crystal due to a high degree of crystallinity and the absence of grain boundaries in the 1-D nanostructured single crystal. It is well known that grain boundaries and other defects act as the recombination sites for electrons and holes.[10]

In addition, the photocatalytic activity of TiO_2 crystals is heavily dependent upon the surface structure (surface atomic arrangement and coordination)[11−14] especially when the particle size is reduced to the nanometer length scale, leading to a large specific surface area. For example, the rutile (100) and (110) facets exhibit lower photoreduction rates toward conversion of Ag^+ to metallic Ag than the (101), (111), and (001) facets.[11] Potentially, photoreduction and photooxidation are predominant on different crystal facets. For instance, the rutile {011} facets provide the metal oxidation sites, while the {110} facets offer the metal reduction sites.[14] Recent investigations have revealed that the anatase TiO_2 nanocrystals with well-faceted {101} surfaces exhibit enhanced photocatalytic activity.[9,15] These studies have shown that the photocatalytic activity of TiO_2 can be tailored by controlling the exposed crystal facets of particles, although the underlying mechanism is not well understood. As of now, the information on the crystal facet effect on photocatalytic activity is limited, because TiO_2 nanocrystals with specific well-faceted surfaces are difficult to obtain. The reports on TiO_2 available in this research area are mainly gained from rutile single crystals,[12] because anatase TiO_2 single crystals with controlled specific well-faceted surfaces are rare in the literature.[16] So far, thin films and bulk TiO_2 single crystals are the major sources for studying the correlation of specific crystal facets with catalysis and the related surface phenomena. Thin films and bulk single crystals provide model systems for fundamental studies but cannot be applied for practical use due to their limited specific surface area.

On the basis of the above discussions, we have designed a uniquely shaped photocatalyst: a single-crystalline anatase TiO_2 (101) nanobelt with the longitudinal dimension on the micrometer scale (or even longer) and the lateral dimension on the nanoscale. Here we present 60−400 nm wide, ∼10 nm thick, and up to 25 μm long nanobelts as an example. Reducing the lateral dimension to the nanometer length scale offers a high specific surface area while keeping the longitudinal dimension of the single crystal on a large scale to minimize the electron−hole recombination rate. The one-dimensionality provides a transport channel and sufficient space for charge separation. Moreover, the unique shape of our developed

nanobelts provides the well-defined anatase (101) facet for two dominantly exposed surfaces. Such anisotropic surface facets could render it highly photoreactivity toward certain chemical species. Therefore, such nanobelts are expected to offer an enhanced photocatalytic activity over sphere-shaped particles with a diameter on the same scale as the lateral dimension of the nanobelts. To the best of our knowledge, we report here for the first time a systematic study on the effects of the shape and the surface structure on the photocatalytic activity of TiO_2 nanobelts. In particular, we present a comparative study of the photocatalytic activities of nanobelts and nanospheres in order to clarify the underlying mechanism of the enhanced photocatalysis performance of the anatase TiO_2 (101) nanobelt photocatalysts.

2. Experimental Methods

Nanobelt Synthesis. The TiO_2 nanobelts were prepared by hydrothermal treatment. Titanium dioxide powder (Alfa Aesar) was added into a 10 M NaOH aqueous solution in a Teflon-lined stainless steel autoclave. The autoclave was sealed and subsequently heated at 200 °C for 24 h. After hydrothermal processing, the white fluffy product was washed with copious deionized water and 0.1 M hydrochloric acid until the pH of the washing solution was reduced to ≤7. The as-washed samples were then calcinated at 700 °C for 30 min at a ramp rate of 1 °C/min. For comparison tests, the TiO_2 nanospheres were purchased directly from Alfa Aesar without further purification.

Material Characterization. The UV−vis absorption spectra were measured under the diffuse reflection mode using a Shimadzu 2550 UV−visible spectrometer equipped with an integrating sphere (UV2401/2, Shimadzu). The photoluminescence (PL) spectra were acquired at room temperature with a Hitachi F-7000 fluorescence spectrophotometer under the ultraviolet excitation of 250 nm. The specific surface area of the particles was measured by the Brunauer−Emmett−Teller (BET) method (Accelerated Surface Area and Porosity System 2020, Micromeritics). The particle morphology was observed with a Hitachi S4700 field-emission scanning electron microscope (SEM). The crystal structure of the TiO_2 particles was characterized by X-ray diffraction (XRD, X'Pert Pro PW3040-Pro, Panalytical Inc.) with Cu Kα radiation, a transmission electron microscope (TEM), high-resolution transmission electron microscopy (HRTEM), and selected area electron diffraction (SAED) (a 200 kV FEI/Philips CM20 TEM apparatus). For TEM sample preparation, the powders were suspended in ethanol, and then a drop of this suspension was deposited onto a holey carbon film supported by a copper grid. The TEM specimen was dried in air prior to the TEM examination.

Photocatalysis Experiments. The photocatalysis experiments were carried out in a commercial photoreactor (LUZ-4 V, Luzchem) equipped with the 148 W UVA lamp (centered at 350 nm, LZC-UVA, Luzchem). A total of 10 mg of TiO_2 catalysts was added to a 10 mL solution of 20 mg/L methyl orange in a 10 mL polyethylene tube. Before irradiation, the suspensions were sonicated in the dark for 5 min. During irradiation, the tubes were placed onto the carousel inside the photoreactor to ensure the even exposure of each tube to the ultraviolet A (UVA) light. At different time intervals of irradiation, the tubes were unloaded and then centrifuged at 10 000 rpm for 1.5 h to separate the supernate and the catalysts. The supernates were collected and analyzed by recording the characteristic absorption peak of methyl orange (464 nm) using a UV−vis spectrometer. According to the calibration plot of the UV absorbance as a function of the remaining methyl orange concentration, the efficiency of the methyl orange decomposition was calculated.

(9) Mor, G. K.; Varghese, O. K.; Paulose, M.; Shankar, K; Grimes, C. A. *Solar Energy Mater. Solar Cells* **2006**, *90*, 2011.
(10) Machlin, E. S. *Materials Science in Microelectronics*; Elsevier: New York, 2005; p 26.
(11) Hotsenpiller, P. A. M.; Bolt, J. D.; Farneth, W. E.; Lowekamp, J. B.; Rohrer, G. S. *J. Phys. Chem. B* **1998**, *102*, 3216.
(12) Pang, C. L.; Thornton, G. *Surf. Sci.* **2006**, *600*, 4405.
(13) Taguchi, T.; Saito, Y.; Sarukawa, K.; Ohno, T.; Matsumura, M. *New J. Chem.* **2003**, *27*, 1304.
(14) Ohno, T.; Sarukawa, K.; Matsumura, M. *New J. Chem.* **2002**, *26*, 1167.
(15) Cho, C. H.; Ho, C. H.; Han, M. H.; Kim, D. H.; Kim, D. K. *Mater. Chem. Phys.* **2005**, *92*, 104.
(16) Yang, H. G.; Sun, C. H.; Qiao, S. Z.; Zou, J.; Liu, G.; Smith, S. C.; Cheng, H. M.; Lu, G. Q. *Nature* **2008**, *453*, 638.

Radical Measurement. Following the approach developed by Uchino et al.,[17] the OH$^{\bullet}$ radicals generated by the TiO$_2$ particles under ultraviolet (UV) irradiation were quantified with an X-band electron spin resonance (ESR) spectroscopy/spin-trapping technique. A suspension of TiO$_2$ particles (100 mg/L) was mixed with a OH$^{\bullet}$ radical spin-trapping agent, 5,5-dimethyl-1-pyrroline-*N*-oxide (DMPO, 100 mM), in the aqueous solution. This solution was kept in the dark for 30 min and then irradiated with the UVA lamps at an emission maximum at 350 nm for 5 min. The ESR spectra were subsequently acquired with an ESR spectrometer at ambient temperature.

DFT Calculations. An *ab initio* tight-binding method, called FIREBALL, which is based on density functional theory with nonlocal pseudopotentials within the local density approximation (LDA),[18] was used to simulate the electronic structure of the anatase TiO$_2$ nanobelts and nanospheres. The confined atomic-like orbitals were used as a basis set for determination of the occupied eigenvalues and eigenvectors of the one-electron Hamiltonian. The calculation was undertaken entirely in real space, which provided substantial computational efficiency. Hamiltonian and overlap matrix elements are precalculated on a numerical grid, and the specific values needed for a particular instantaneous conformation are extracted from the tabulated values via interpolation. Naturally, the integral tables need to be generated only once, for a given set of atomic species, rather than performing quadratures "on the fly" during a molecular dynamics (MD) run. In the calculations, a minimal basis set for O and Ti was chosen with the addition of an excited *p*-state for polarization to the Ti ground-state configuration. This method has been successfully used for obtaining geometries and electronic properties of bulk TiO$_2$ material and TiO$_2$ nanostructures.[19,20] For the simulations reported here, the atomic structure of the nanobelts and nanospheres were carved out from anatase structure. For each nanostructure, the stoichiometry was preserved and no saturation of dangling bonds or charge embedding was applied. The initial geometries were fully relaxed to the nearest local minimum structure.

Since the transport mobility of the charge carriers in the anatase TiO$_2$ lattice is linearly related to conductivity, one can estimate the conductivity. It was reported[21,22] that the Kubo−Greenwood formula built the natural approximate connection between the conductivity and the electronic states (localized states) and energies. Hence the Kubo formalism in conjunction with *ab inito* methods in FIREBALL was used to estimate the dc conductivity in the TiO$_2$ nanobelts and the nanospheres. The dc conductivity was computed from trajectory averaged quantities using the formulas developed by Abtew et al.[23] The well-relaxed models of TiO$_2$ nanobelts and nanospheres were used in the present work. The models were prepared at room temperature ($T = 300$ K) for a total time of 15.0 ps. Once the models were well equilibrated, a constant-temperature molecular dynamic simulation for 2000 steps (with the time step of 1.50 fs) was performed where data were collected after every 10 steps to obtain the average dc conductivity. During the calculation, the MD simulations were carried out in the NVT ensemble (i.e., the number of particles *N*, the volume *V*, and the temperature *T* of the system are kept constant).

3. Results and Discussions

The BET adsorption analysis showed that the specific surface areas of the nanobelts and the nanospheres were 20.83 and 57.70 m^2/g, respectively. Both the as-synthesized titania nanobelts and the commercial titania nanospheres exhibited the monolithic anatase phase, as confirmed by the XRD patterns (Figure S1 in Supporting Information). The morphology of the nanospheres is revealed in Figure S2. The nanospheres are around 150 nm in diameter. Figure 1a shows the SEM image of the nanobelts. The nanobelts are 60−400 nm wide and ∼10 nm thick. The length of the nanobelts varies from several micrometers to 30 μm. Figure 1b shows a bright-field TEM image taken from a single nanobelt that is about 180 nm wide and about 10 nm thick as determined from the TEM images observed from different directions. Electron diffraction data indicate that the nanobelts are single crystalline anatase TiO$_2$ (tetragonal $a = 0.3785$ nm, $c = 0.9415$ nm). After the correction of the relative rotation between the image and the diffraction pattern, the growth direction of the nanobelt is determined to be [010]. This is supported by the high-resolution TEM image in Figure 1c, where the lattice fringes perpendicular to the growth direction has a spacing of 0.38 nm, which is equal to the lattice parameter in the [010] direction. In addition, the crystallographic plane of two major exposed surfaces of the nanobelts is determined to be the (101) facet, as shown in Figure 1d, which is the most thermodynamically stable crystal facet of anatase TiO$_2$.[24] The details of the crystallographic plane identification can be seen in the Supporting Information.

The photocatalysis performance was evaluated in terms of the decomposition rate of methyl orange in an aqueous solution catalyzed by the TiO$_2$ nanoparticles under ultraviolet (UV) A irradiation. Although the specific surface area of the nanospheres was about 2.8 times that of the nanobelts, the nanobelts exhibited better photocatalytic activity than the nanospheres (Figure 2). In order to clarify the underlying mechanism of the enhanced photocatalytic activity of the anatase TiO$_2$(101) nanobelts, we have investigated how the shape and the surface structure of the nanobelts affect the following four processes in photocatalysis: (a) light-irradiation-induced formation of conduction band electrons and valence band holes; (b) transfer of the photogenerated electrons and holes to the photocatalyst surface; (c) trapping of the photogenerated charge carriers at the photocatalyst surface and formation of reactive oxygen species (ROS); and (d) recombination of electron−hole pairs.

(a) Light Absorption. Figure 3 shows the UV−visible spectra of the TiO$_2$ nanobelts and the nanospheres. Under ultraviolet irradiation, electrons in the valence band absorb the photon energy and jump to the conduction band, leaving holes in the valence band. Light absorption is mainly determined by the band structure and the dipole matrix elements. It is deduced from Figure 3 that the bandgaps of the nanobelts and the nanospheres are almost identical (3.4 eV). Given their similar specific surface area, no evident difference in the light absorption efficiency was observed between the nanobelts and the nanospheres.

(b) Transfer of Electrons and Holes to the Photocatalyst Surface. Mobility of charge carriers in TiO$_2$ is one of the important factors that govern the photocatalysis efficiency. For example, although anatase TiO$_2$ has a larger bandgap than rutile, it is more photoactive than rutile. One of the major reasons is that the electron mobility in anatase is 40 times greater than

(17) Uchino, T.; Tokunaga, H.; Ando, M.; Utsumi, H. *Toxicol. in Vitro* **2002**, *16*, 629.

(18) Lewis, J. P.; Glaesemann, K. R.; Voth, G. A.; Fritsch, J.; Demkov, A. A.; Ortega, J.; Sankey, O. F. *Phys. Rev. B* **2001**, *64*, 195103.

(19) Wang, H.; Lewis, J. P. *J. Phys.: Condens. Matter* **2006**, *18*, 421.

(20) Tafen, D. N.; Wang, J.; Wu, N. Q.; Lewis, J. P. *Appl. Phys. Lett.* **2009**, *94*, 093101.

(21) Kubo, R. *J. Phys. Soc. Jpn.* **1957**, *12*, 570.

(22) Greenwood, D. A. *Proc. Phys. Soc.* **1958**, *71*, 585.

(23) Abtew, T. A.; Zhang, M.; Drabold, D. A. *Phys. Rev. B* **2007**, *76*, 045212.

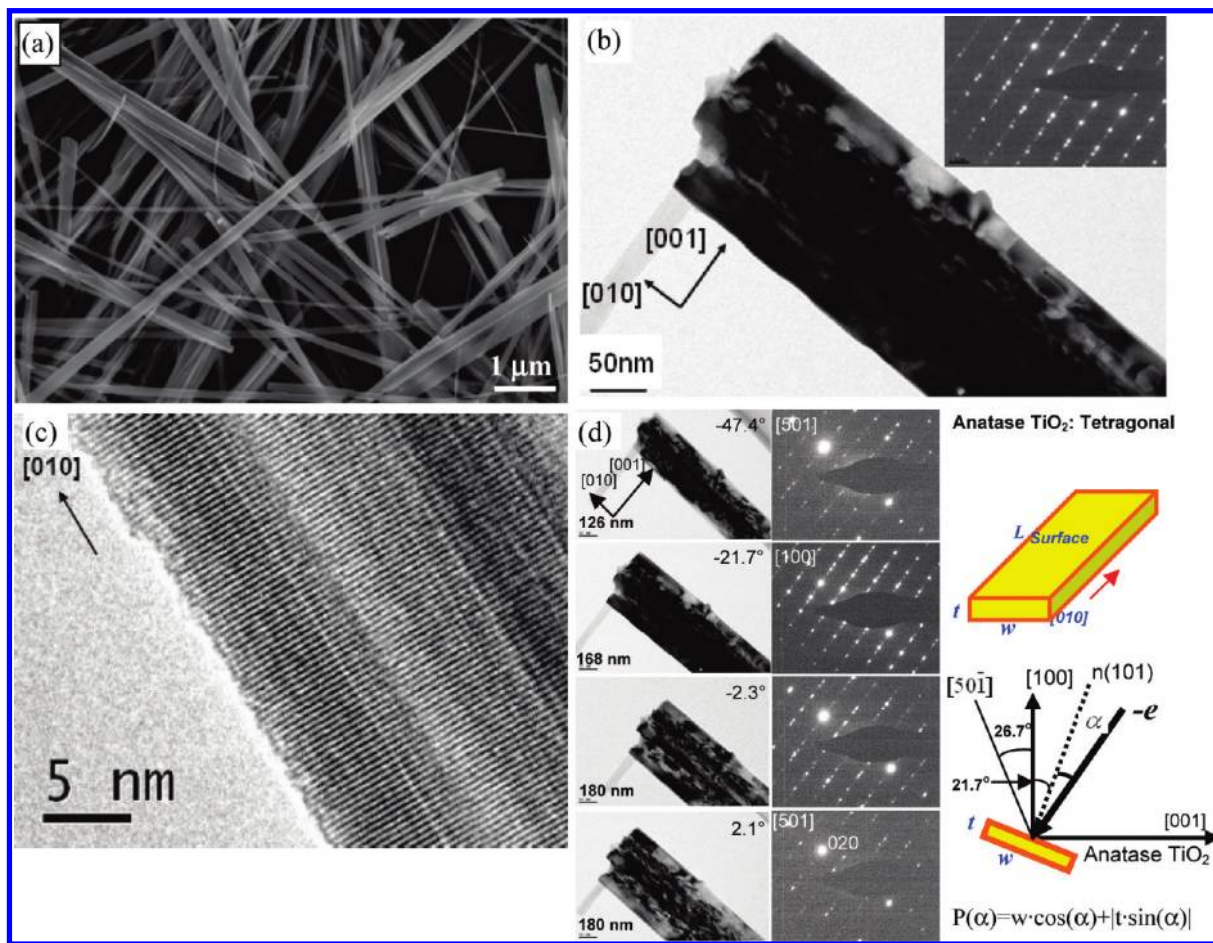(24) Lazzeri, M.; Vittadini, A.; Selloni, A. *Phys. Rev. B* **2001**, *63*, 155409.

Figure 1. (a) SEM images of the anatase TiO_2 nanobelts; (b) bright-field TEM image of a TiO_2 nanobelt; the inset is a selected area electron diffraction (SAED) pattern taken along the [100] direction of the nanobelt; (c) HRTEM image of a nanobelt; (d) bright-field TEM images and corresponding SAED patterns of a TiO_2 nanobelt recorded in different crystallographic orientations while keeping the [010] axis horizontal, as well as schematic illustrations of the nanobelt and the relationship between the incident beam and the nanobelt while taking images and diffraction patterns.
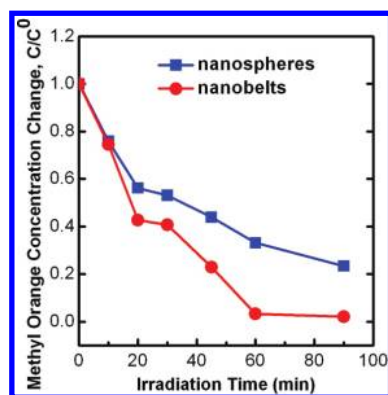
Figure 2. Degradation of methyl orange in an aqueous solution by the TiO_2 nanobelts and the nanospheres as a function of exposure time to UV irradiation.
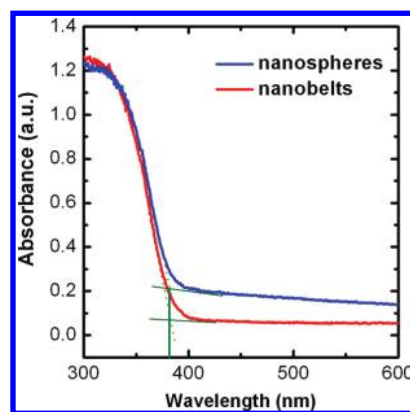

Figure 3. Diffuse reflectance UV−visible spectra of the TiO_2 nanobelts and the nanospheres.

that in rutile.[25,26] Localized states lie within the mobility gap, and their localization can impede the transfer of charge carriers to the reactive sites at the photocatalyst surface. To examine the mobility, the electronic density of states of the TiO_2

nanoparticles was calculated by FIREBALL. For a particular electronic state, the number of accessible atoms, W, describes the spatial extent of that state.[27] W gives a quantitative measure of the number of atoms that a particular state reaches. The smaller the W, the more localized the state. Figure 4 shows the states near the band edges of the nanobelts are less localized as compared to those in the nanospheres. In addition, localized

(25) Kera, Y.; Kominani, H.; Murakami, S. *Photocatalysis: Science and Technology*; Kaneko, M., Okura, I., Eds.; Kodansha, Springer: Tokyo, 2002; pp 29−49.
(26) Voinuv, M.; Augustynkim, J. *Heterogeneous Photocatalysts*; Schiavello, M., Ed.; John Wiley and Sons: New York, 1997; pp 1−42.

(27) Lewis, J. P.; Cheatham, T. E.; Starikov, E. B.; Wang, H.; Sankey, O. F. *J. Phys. Chem. B* **2003**, *107*, 2581.
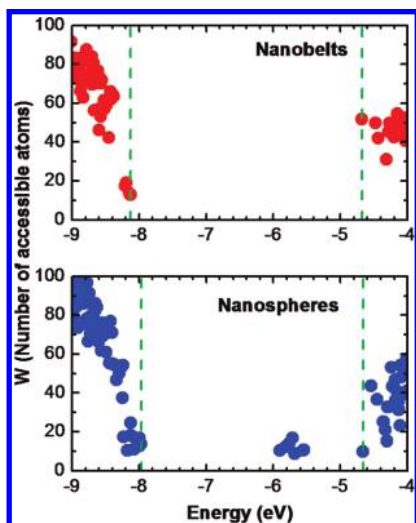
Figure 4. Number of accessible atoms (*W*) for each electronic state near the valence and conduction band edges of the nanobelts and nanospheres. Note that the smaller the *W*, the more localized the state. The dashed lines indicate the valence and conduction band edges.

states are absent in the bandgap of the nanobelts while present in the nanospheres. The ultraviolet light could excite the electrons from both the valence band and the localized midgap states to the conduction band, leaving the holes behind. These states in the midgap act as the traps for the photogenerated holes and consequently act as the recombination centers. As a result, these holes in the midgap will have very low mobility. In contrast, the holes in the valence band are expected to have larger mobility, which can be transferred to the catalyst surface to directly oxidize the preadsorbed species.

In addition, the transport mobility of the charge carriers in the TiO₂ lattice was also calculated by the DFT method to quantitatively evaluate the capability of transporting charge carriers to the particle surface. Since the mobility is linearly related to the conductivity, one can estimate the conductivity, which is much easier to calculate. The natural approximate connection between the conductivity and the electronic states (localized states) and energies was considered to estimate the dc conductivity in the TiO₂ nanobelts and the nanospheres.[21,22] At room temperature the dc conductivity was estimated to be on the order of $\sim 10^{-7}\ \Omega^{-1} \cdot cm^{-1}$ for the nanobelts and $\sim 10^{-9}\ \Omega^{-1} \cdot cm^{-1}$ for the nanospheres. Our results give a crude estimation of the carrier transport in the nanostructures and show that the conductivity of the nanobelts is far greater than that of the nanospheres. Given that the conductivity is tied to the mobility, our results suggest that the carrier mobility in the nanobelts is much higher than that in the nanospheres.

(c) Trapping of Charge Carriers at the Surface and Formation of Reactive Oxygen Species. Photogenerated charge carriers can react with electron donors or acceptors adsorbed on the surface of photocatalysts.[1–3,28–30] Typically, for photocatalysts in an aqueous solution, the photogenerated valence band holes interact with chemisorbed OH⁻ or H₂O to form surface-bound hydroxyl radical (OH•) and the conduction band electrons react with adsorbed O₂ to form superoxide radical ($O_2^{\bullet-}$).[31–33] In the early studies, the hydroxyl radical[1,2] is
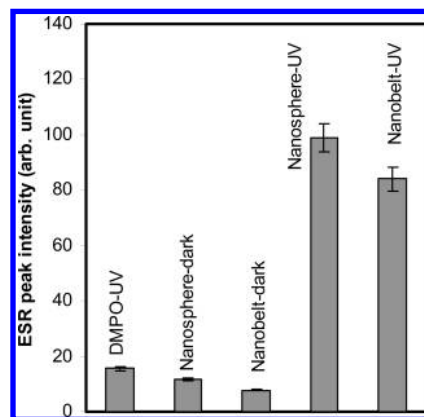

Figure 5. Peak intensity of the ESR spectra obtained from the DMPO solution, the TiO₂ nanosphere−DMPO solution, and the nanobelt−DMPO solution before and after UVA irradiation, indicating the amount of hydroxyl radical (OH•) photogenerated under different conditions.

considered as the main oxidative species responsible for the oxidation of organics, although some reactions can also be initiated by direct hole oxidation, especially when the adsorption of the substrate is extensive and the concentration of substrate is relatively high.[34] In recent studies, the superoxide radical has also been found to offer another reaction pathway for oxidative degradation of organics.[2,3,34–37] When TiO₂ is subject to light irradiation, electrons are excited from the valence band into the conduction band. It has been reported that adsorbed oxygen molecules act as the electron scavengers and combine with the electrons from the conduction band to form superoxide anions in air or in air-saturated water.[38–41] The concentration of superoxide increases with increase in the O₂ concentration. This indicates that during photocatalytic reactions photogenerated electrons are mainly trapped by adsorbed oxygen molecules, leading to the formation of superoxide.[40] The superoxide radical anion acts as an intermediate that can be involved in the oxidization of organics.[40,41]

In the present study, the amount of photogenerated OH• radical by the TiO₂ particles upon UV illumination in the aqueous solution was determined by the ESR signal intensity of the DMPO−OH• adduct (Figure 5). ESR measurements gave direct evidence that the hydroxyl radicals were involved in the photocatalysis process. It was found that the nanobelts generated slightly less hydroxyl radicals than the nanospheres even though the nanobelts exhibited higher photocatalytic activity toward the decomposition of methyl orange. Therefore, it is deduced that decomposition of methyl orange was not solely via the oxidation of methyl orange by the hydroxyl radical.

Therefore, it is necessary to examine the role of superoxide radical in the photoctalysis. Superoxide radical has been reported

(28) Berger, T.; Sterrer, M.; Diwald, O.; Knzinger, E.; Panayotov, D.; Thompson, T. L; Yates, J. T. *J. Phys. Chem. B* **2005**, *109*, 6061.
(29) Henderson, M. A.; Epling, W. S.; Peden, C. H. F.; Perkins, C. L. *J. Phys. Chem. B* **2003**, *107*, 534.
(30) Panayotov, D.; Yates, J. T., Jr. *Chem. Phys. Lett.* **2003**, *381*, 154.
(31) Remillard, J. T.; McBride, J. R.; Nietering, K. E.; Drews, A. R.; Zhang, X. *J. Phys. Chem. B* **2000**, *104*, 4440.
(32) Ishibashi, K.; Fujishima, A.; Watanabe, T.; Hashimoto, K. *J. Phys. Chem. B* **2000**, *104*, 4934.
(33) Peiro, A. M.; Colombo, C.; Doyle, G.; Nelson, J.; Mills, A.; Durrant, J. R. *J. Phys. Chem. B* **2006**, *110*, 23255.
(34) Kim, S.; Park, H.; Choi, W. *J. Phys. Chem. B* **2004**, *108*, 6402.
(35) Schwitzgebel, J.; Ekerdt, J. G.; Gerischer, H.; Heller, A. *J. Phys. Chem.* **1995**, *99*, 5633.
(36) Cermenati, L.; Pichat, P.; Guillard, C.; Albini, A. *J. Phys. Chem. B* **1997**, *101*, 2650.
(37) Wang, Y.; Hong, C. S. *Water Res.* **2000**, *34*, 2791.
(38) Chatterjee, D.; Mahata, A. *Appl. Catal., B* **2001**, *33*, 119.
(39) Ishibashi, K.; Fujishima, A.; Watanabe, T.; Hashimoto, K. *J. Phys. Chem. B* **2000**, *104*, 4934.
(40) Kwon, B. G. *J. Photochem. Photobiol. A* **2008**, *199*, 112.
(41) Fox, M. A.; Chen, C. C. *J. Am. Chem. Soc.* **1981**, *103*, 6757.

to be formed via the adsorption of molecular O_2 on the TiO_2 surface in an aqueous solution and subsequent trapping of the photogenerated electrons.[42,43] Trapping of photogenerated electrons by molecular O_2 can affect the photocatalysis efficiency in two ways. In a direct way, the photoreduced superoxide radical anion acts as an intermediate that can be involved in the oxidization of organics.[40,41] In an indirect way, capture of the photogenerated electrons enables the accumulation of more reactive holes.[44,45] Even for a reaction photocatalyzed via the hydoroxyl radicals, it is coupled with reduction of dissolved O_2 initially to peroxide and ultimately to water. The rate of hydroxyl radical- (or hole-) initiated oxidation cannot be faster than that of O_2 reduction by the photogenerated electrons. When O_2 is not reduced at a sufficiently high rate, the electrons accumulate on the photocatalyst and consequently increase the rate of radiationless electron−hole recombination. In this case, the rate of photooxidation is limited by the rate of O_2 reduction.[44,46,47] Hence the role of molecular O_2, a strong electron scavenger, in the photocatalysis process was examined. The decomposition reaction of methyl orange, which was photocatalyzed by the TiO_2 nanobelts and the nanospheres, proceeded in the aqueous solution under ambient air, the O_2-saturated conditions, and the N_2-saturated conditions, respectively. For the decomposition reaction of methyl orange catalyzed by the nanobelts, the photocatalysis rate was enhanced when the aqueous solution was saturated with O_2 by bubbling oxygen gas into the solution, while the photocatalysis rate was reduced under the N_2-saturated condition (Figure S3a). In contrast, switching from the O_2-rich to the O_2-deficient condition had little effect on the rate of the reaction photocatalyzed by the nanospheres (Figure S3b). These results suggest that adsorption and photoreduction of molecular O_2 on the TiO_2 nanobelt surface could be different from that on the nanosphere surface due to the difference in the shape and surface structure.

The adsorption and photoreduction of oxygen molecules on the nanobelt and nanosphere surfaces were further investigated using the FIREBALL simulation. For the anatase TiO_2 nanobelts, the two dominant surfaces are terminated by the (101) crystal plane. Therefore, it is reasonable to consider only the (101) facet in our calculations. The lattice parameters adopted in this calculation were compared with the experimental result in ref 16, which has proved that FIREBALL is able to generate the correct lattice constants for the anatase TiO_2 unit cell. The (101) facet was modeled using a slab by adding 20 Å of vacuum to a 384-atom bulk supercell containing eight TiO_2 layers. In this supercell, the geometry has been optimized by relaxing all the atomic positions without fixing any atoms on the bottom of the slab. Figure 6a shows the relaxed clean anatase TiO_2 (101) surface. The surface exposes 5-fold ($5c$) and 6-fold ($6c$) coordinated Ti atoms, as well as 2-fold ($2c$) and 3-fold ($3c$) coordinated O atoms. The calculated surface energy is 0.81 J/m^2, which is in good agreement with that calculated by Lazzeri et al.[24] The nanosphere is cut from a perfect bulk anatase supercell
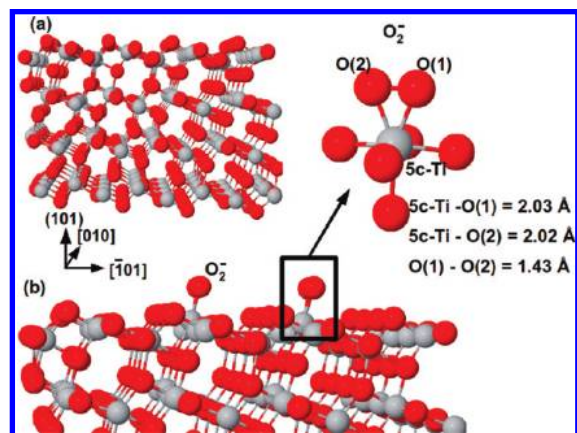

Figure 6. Optimized geometries of (a) anatase (101) TiO_2 surface of the nanobelts; (b) O_2^- molecule absorbed at the 5-fold coordinated Ti site on the surface. Note: Superoxide O_2^- is added from the beginning by adding an extra electron to the system.
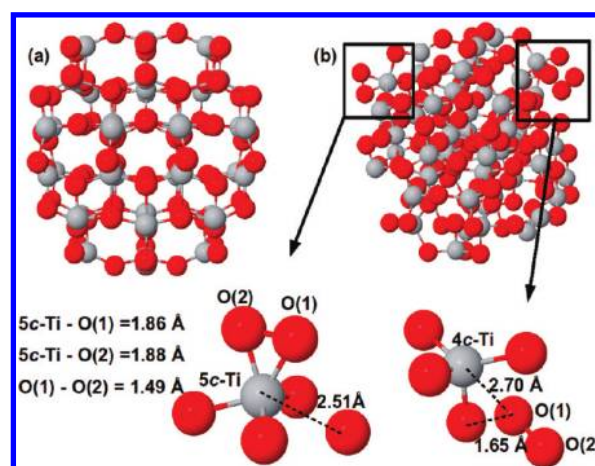

Figure 7. Optimized geometries of (a) anatase TiO_2 nanosphere; (b) O_2^- molecule absorbed at the 5-fold coordinated Ti site on a surface.

and put into a 100 Å vacuum box, with the origin placed at the center of mass of the sphere. Some of the surface oxygen or titanium atoms are removed to ensure electroneutrality. During the optimization the diameter of the nanosphere increases from 1.5 to 1.8 nm (Figure 7a). The relaxed structure shows significant structural disorder on the surface of the nanosphere, with the presence of both undercoordinated Ti and O atoms. Besides the nanosphere with 144 atoms in this work, we have also carried out a series of calculations of anatase nanospheres with the size scale from 1.5 to 2.5 nm.[48] These calculations have shown that anatase nanopheres present significant structural disorder on the surfaces after optimization. The surface of the nanosphere shows the presence of 5-fold ($5c$), 4-fold ($4c$), and 3-fold ($3c$) coordinated Ti atoms, as well as 3-fold ($3c$) and 2-fold coordinated ($2c$) O atoms. It should be noted that the number of $5c$-Ti sites is identical for the nanobelt (101) facet and the nanosphere. We estimate the strength of a molecule−surface interaction through the calculation of desorption enthalpies, ΔH_{des}.

Figure 6b shows the optimized geometry of an O_2^- anion-molecule absorbed on a $5c$-Ti site. The structure and geometry are in good agreement with that obtained by Mattioli et al.[43] In the O_2^- anion-molecule the two O atoms are both bonded to the $5c$-Ti surface atom in a symmetric configuration with equal Ti−O distances, 2.02 Å, close to that in the bulk anatase. The formation of these two strong Ti−O

(42) Nakamura, R.; Imanishi, A.; Murakoshi, K.; Nakato, Y. *J. Am. Chem. Soc.* **2003**, *125*, 7443.
(43) Mattioli, G.; Filippone, F.; Bonapasta, A. A. *J. Am. Chem. Soc.* **2006**, *128*, 13772.
(44) Wang, C. M.; Heller, A.; Gerischer, H. *J. Am. Chem. Soc.* **1992**, *114*, 5230.
(45) Brezova, V.; Stasko, A.; Lapcik, L., Jr. *J. Photochem. Photobiol. A* **1991**, *59*, 115.
(46) Berger, T.; Sterrer, M.; Diwald, O.; Knçzinger, E. *Chem. Phys. Chem.* **2005**, *6*, 2104.
(47) Henderson, M. A.; White, J. M.; Uetsuka, H.; Onishi, H. *J. Catal.* **2006**, *238*, 153.

(48) Wang, H.; Lewis, J. P. *J. Phys. Chem. C* **2009**, *113*, 16631.

bonds is confirmed by the value of the energy required to detach the ion-molecule from the surface, $\Delta H_{des} = -1.54$ eV. The absorbed O_2 molecule induces an acceptor electronic level in the energy gap, where the occupying electrons are mainly localized on the O_2 molecule. The presence of an acceptor close to the valence band maximum indicates that an electron transfer can easily occur from the surface to the molecule by forming an O_2^- radical, which is difficult to detach from the surface.

For the nanosphere, one O_2^- ion-molecule was initially placed on the surface at a distance of 2.1 Å above one of the 5c-Ti sites of the nanosphere surface. During relaxation and molecular dynamics run, the molecule continuously changed its orientation, dissociated from the 5c-Ti sites, moved away from the surface, and formed a weak bond with a 4c-Ti atom. This result is supported by the fact that the Ti–O distance between the Ti surface atom and one of the O atoms of the molecule was 2.70 Å, while the Ti–O bond distance in the bulk was about 2.0 Å. In addition, the estimated energy to detach the O_2^- ion from the surface of the nanosphere was -0.53 eV. Next, two O_2^- anion-molecules were placed on the surface of the nanosphere. After geometry optimization, one of the molecules moved away from the surface to form a weak bond with a 4c-Ti atom, and the other did not dissociate from the 5c-Ti site. Instead there was a breaking of the bond between the weakly coordinated 3c-O and the 5c-Ti atoms involved in the adsorption (see Figure 7b). The two oxygen atoms are both bonded symmetrically to the 4c-Ti atom with Ti–O distances of 1.88 and 1.86 Å. These bonds are shorter than those in the bulk anatase. The O–O distance in the final configuration is 1.49 Å. These results are similar to that obtained by Mattioli et al. for the absorbed O_2^{-2} anion-molecule on the anatase TiO_2 (101) surface.[43]

The above results show that the O_2 molecule–surface bonding is significantly strengthened by the capture of one electron on the anatase (101) facet of the TiO_2 nanobelt, whereas the O_2 molecule–surface bonding is weakened in the nanosphere. As a direct consequence, the single-crystalline nanobelts with the (101) facet have a better capability of generating superoxide radical as compared to the nanospheres. As discussed above, promotion of the superoxide radical formation on the TiO_2 surface improves the photocatalysis efficiency. Since the (101) facet dominates the surface structure of the nanobelts, higher reactivity of oxygen molecules on the (101) facet is believed to be one of the origins of the enhanced photocatalytic activity of the nanobelts over the nanospheres.

(d) Recombination of Electron–Hole Pairs. The photocatalysis efficiency is determined by the competition between the charge separation process and the charge recombination process, both in the bulk and on the surface. Photoluminescence spectra can be used to evaluate the charge recombination rate as reported in the previous studies,[49,50] because PL spectra directly arise from the radiative recombination processes of the electrons and the holes between two different energy states. Thereore, the PL spectra were obtained from the TiO_2 nanobelts and the nanospheres, respectively (Figure S4 in Supporting Information). The peak centered at around 365 nm in the PL spectra was attributed to the emission of the bandgap transition.[51] The peaks around 470 nm and around 550 nm were ascribed to the emissions from the charge transfer transition of oxygen vacancy trapped electrons.[49,52,53] The higher the PL emission intensity, the higher the recombination rate of the photogenerated electrons and holes. Figure S4 suggests that the nanobelts have a lower recombination rate than the nanospheres. The lower electron–hole recombination rate of the nanobelts originates from the following factors: (i) the charge carriers have higher mobility in the nanobelts than in the nanospheres; (ii) the single-crystal nature along the longitudinal dimension of the nanobelts provides a large space as the pathway for charge separation, while the nanospheres are confined by the space; (iii) the anatase nanobelts with two dominant surfaces terminated by the (101) facet have higher reactivity with molecular O_2 than the nanospheres. More superoxide anions are formed by trapping the photogenerated electrons on the (101) faceted nanobelts. Thus more charge carriers are spatially separated on the nanobelt surface.

4. Conclusions

Although the TiO_2 nanobelts and the nanospheres possessed the same phase structure, similar specific surface area, and similar photoadsorption efficiency, the nanobelts exhibited better photocatalytic activity than the nanospheres. The nanobelts possessed higher charge carrier mobility and provided the pathway for transport of charge carriers throughout the longitudinal direction, which was expected to facilitate the charge separation. Our results indicate that the geometric shape of the nanocrystal is an important factor in the catalyst design besides the specific surface area. Single-crystalline one-dimensional (nanobelts, nanowires, and nanotubes) or two-dimensional (nanosheets) nanostructures are expected to show higher photocatalytic activity than zero-dimensional nanocrystal counterparts. The nanobelts showed an enhanced reactivity with O_2 molecules on the (101) facet, leading to more superoxide anions ($O_2^{\bullet-}$) on the photocatalyst surface. Generation of superoxide anions was a process of trapping the photogenerated electrons, which promoted the charge separation and resulted in a lower electron–hole recombination rate. Our work suggests that photocatalysis efficiency can be improved by tailoring the surface crystal structure.

Supporting Information Available: XRD patterns of the TiO_2 nanobelts and nanospheres are presented in Figure S1. The SEM image of the TiO_2 nanospheres is shown in Figure S2. Degradation of methyl orange in an aqueous solution saturated with oxygen, nitrogen, and air is shown in Figure S3. Photoluminescence spectra of the TiO_2 nanobelts and the nanospheres are presented in Figure S4. Method for determining the facet of two major exposed surfaces of the nanobelts is also shown. This material is available free of charge via the Internet at http://pubs.acs.org.

JA909456F

(49) Li, D.; Haneda, H.; Hishita, S.; Ohashi, N. *Chem. Mater.* **2005**, *17*, 2596.
(50) Cong, Y.; Zhang, J.; Chen, F.; Anpo, M. *J. Phys. Chem. C* **2007**, *111*, 6976.
(51) Li, F. B.; Li, X. Z. *Chemosphere* **2002**, *48*, 1103.
(52) Lei, Y.; Zhang, L. D.; Meng, G. W.; Li, G. H.; Zhang, X. Y.; Liang, C. H.; Chen, W.; Wang, S. X. *Appl. Phys. Lett.* **2001**, *78*, 1125.
(53) Serpone, N.; Lawless, D.; Khairutdinov, R. *J. Phys. Chem.* **1995**, *99*, 16646.